Physica E 63 (2014) 36–44

Contents lists available at ScienceDirect

Physica E

journal homepage: www.elsevier.com/locate/physe

Model of electron tunneling coupled to torsional vibrations: Exact solution and study of performance of approximation methods

Lukáš Gráf, Martin Čížek*

Charles University in Prague, Faculty of Mathematics and Physics, Institute of Theoretical Physics, V Holešovičkách 2, 180 00 Praha 8, Czech Republic

HIGHLIGHTS

- A 2D model of the electron interaction with molecular vibrations is solved.
- Various transmission functions are calculated accurately numerically.
- The exact results are compared with various approximations.
- The validity of approximations is discussed.
- The excitation of the vibrational degree of freedom is detailed.

ARTICLE INFO

Article history:
Received 7 January 2014
Received in revised form
3 May 2014
Accepted 6 May 2014
Available online 14 May 2014

Keywords:
Molecular junction
Resonance
Electron transport

ABSTRACT

A two dimensional model for the electron interaction with molecular vibrations in molecular junctions is proposed. Alternatively the model can be applied to tunneling through a cylindrical nano-structure. The transmission function is calculated accurately numerically. The exact results are then compared with various approximations: (1) completely frozen vibrations for very light molecule, (2) Chase approximation for very heavy molecule, and (3) discrete-state-in-continuum model in resonant regime. The validity of these approximations is discussed in terms of the characteristic time-scales and coupling strengths. The excitation of the vibrational degree of freedom and the emergence of prominent threshold structures in the strong coupling regime are discussed in more details.

1. Introduction

Molecular electronics is promising field of research that may lead not only to ultimate miniaturization of the electronic devices but also to complete change of paradigm in the chip production [1]. Prototypical device for study of the conductive properties of individual molecules is represented by molecular junction, which consists of two microscopic electrodes bridged by single molecule, covalently bonded to the electrodes. First such device has been constructed in late 90s [2]. Since then this field of research substantially advanced considering both the experimental techniques and theoretical methods to describe such devices (see for example [3,4] for recent reviews).

Calculation of the current conduction properties of a molecular junction represents a great challenge for the theory (see for example [5–7] for reviews). The theory is even more challenging when the vibrational degrees of freedom of the molecule are taken into account (see for example [8–13]).

One of the key difficulties is the many-particle nature of the current conduction in the junction due to the presence of Fermi sea of electrons. It is usually treated with the nonequilibrium-Green's function formalism considering the electron–vibrational coupling as a perturbation [8]. We take different point of view by considering the current conduction as a sequential scattering of individual electrons through the junction [14,15]. Although this approximation does not take into account the coupling of electrons within the Fermi sea correctly it allows us to concentrate on the difficulties due to the coupling of the electronic and the vibrational motion. In our model, we do not have to restrict neither to a small values of vibrational coupling nor to harmonic vibrations like in the most of the studies of molecular junctions.

This approximation also links the problem of theoretical description of the molecular junction to the theory of electron scattering from the molecules in gas phase [16,17].

There are number of approximations used to treat the problem of vibrations of the molecules in the molecular junction and their interaction with electronic degrees of freedom. First, in many calculations the vibrations are completely ignored. The authors just assume that the atoms in the molecule are sitting in their equilibrium positions and do not move. This may be good approximation if the

* Corresponding author.
E-mail address: Martin.Cizek@mff.cuni.cz (M. Čížek).

http://dx.doi.org/10.1016/j.physe.2014.05.008
1386-9477/

electron-transport properties of the molecule are not much influenced by the position of the atoms. The simplest approximation including vibrations takes the positions of the atoms fixed on the first place, but then averages the transmission function of the junction over vibrational wave-functions of the molecules. In the context of electron-molecule scattering this approach is known as Chase or adiabatic-nuclei approximation [18,16]. The same approach is also used in the molecular electronics calculations (see for example [19]).

Another frequently used approach is based on the projection-operator formalism of Feshbach [20,16]. It assumes that the electron can only get through the junction through a localized state, which is usually called the discrete state. The electron dynamics is thus reduced to a model of the discrete state in continuum which is coupled to vibrational dynamics. This is very powerful approach in some cases [16], but it is rarely used in the full form, because it leads to nonlocal, energy-dependent effective term in the effective interaction. This nonlocal term is often replaced by local complex potential (LCP) [16,21], which is computationally much easier to handle. This approximation is usually called wide band limit in context of solid state physics.

In this paper we propose simple exactly solvable model for the transmission of an electron through a molecular junction, where it can interact with one vibrational degree of freedom. The model is introduced in the following paragraph. The method of exact solution of the dynamics and the formula for the transmission function are presented in Section 2. Section 3 is devoted to discussion of resulting transmission function. We stress the understanding of the physics behind the structures observed in the transmission functions and their description in various approximation methods mentioned above. Since we have exact solution in our model the present paper can serve as a benchmark for the performance of the approximation methods in various transport regimes. We conclude with Section 4 summarizing the results and suggesting further extension of the present approach in the future.

1.1. Description of the model

A simple model to mimic the behavior of an inelastic electron tunneling through a molecular junction is introduced here. The system we have in mind is schematically represented in Fig. 1. A molecule capable of the torsional vibrational motion is captured between two electrodes. We consider a motion of a single electron, which is freely moving inside the electrodes. It can also jump to the molecule through a potential barrier either from the left or from the right electrode. The strength of the barrier is assumed to depend on the orientation of the molecule in the junction. Such system is described with the model hamiltonian

$$H = -\frac{1}{2m_e}\frac{\partial^2}{\partial x^2} - \frac{1}{2I}\frac{\partial^2}{\partial \varphi^2} + \lambda_L(\varphi)\delta(x+a) + \lambda_R(\varphi)\delta(x-a), \tag{1}$$

where the coordinate x describes the linear motion of the electron through the junction and the coordinate φ is the torsional angle for the molecule. The mass of the electron m_e and the offset of the barriers a can be eliminated by scaling of the coordinate x and the energy. We thus set $m_e = a = 1$. The coordinate $\varphi \in (0, 2\pi)$ cannot be scaled and the moment of inertia of the molecule I is an important parameter influencing the character of the behavior of the system.

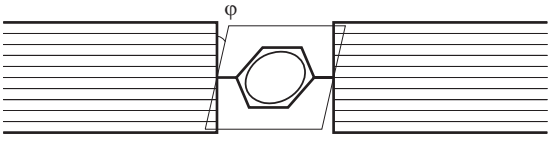

Fig. 1. A schematic representation of the molecular junction with a torsional vibrational mode.

The strength of the barrier between the molecule and the left/right electrode is $\lambda_L(\varphi)$ and $\lambda_R(\varphi)$ respectively. Its φ-dependence drives the coupling of the electronic and the vibrational motion.

To keep the model simple we assume that the φ-dependence is given by two lowest terms in the Fourier series expansion

$$\lambda_l = \alpha_l + \beta_l \cos(\varphi - \varphi_l), \tag{2}$$

where $l = L, R$ and α_l, β_l, φ_l are real constants. The constant α thus controls the strength of the barrier, the ratio $v = \beta/\alpha$ the strength of the electron–vibration coupling and the difference $\varphi_0 = \varphi_R - \varphi_L$ the asymmetry of the junction (we can set $\varphi_L = 0$ without loss of generality). The assumption (2) is motivated by the behavior of the coupling in the molecules consisting of several benzyl rings. The cosine term results from the overlap of two π-orbital systems [22–25]. The suggested coupling functions λ_l correspond to the situation, where the part of the molecule undergoing the torsional motion is connected to the electrodes through additional benzyl rings.

There is an alternative interpretation of the model just described. The same model hamiltonian describes a motion of an electron on the surface of a cylinder with two barriers that break the axial symmetry. The coordinates x and φ parameterize the surface of the cylinder. The moment of inertia $I = m_e R^2$ depends on the radius R of the cylinder. The hamiltonian (1) can thus be understood as the description of the electron tunneling through a cylindrical nano-structure with double barrier. This alternative interpretation of the model is schematically represented in Fig. 2.

Before explaining the method of the solution of the electron scattering through the junction, we would like to discuss briefly the relevant parameter ranges. The parameter I gives the moment of inertia in units $m_e a^2$. In realistic molecular junctions we expect the values of the order of $10^3 - 10^4$. If the model is interpreted as an electron tunneling through the nano-structure (Fig. 2), the value of I can be tuned arbitrarily depending on the aspect ratio of the device. Another important parameters are the strength of the barriers α_l and the vibrational coupling strength $v = \beta/\alpha$. Since the nature of the bonding of a molecule to the electrodes can vary from strong covalent bond to very loose or no bonding (tunneling setup), these values can also be tuned quite freely to investigate different transport regimes.

2. Full numerical solution of the problem

The problem of the single electron transmission through the double barrier described by model hamiltonian (1) can be solved by applying the scattering boundary conditions to a corresponding stationary Schrodinger equation. We will rather employ the scattering theory formalism based on the splitting of the Hamiltonian (1) into the kinetic and the potential energy terms

$$H = H_0 + V,$$
$$H_0 = -\frac{1}{2}\frac{\partial^2}{\partial x^2} - \frac{1}{2I}\frac{\partial^2}{\partial \varphi^2},$$
$$V = \lambda_L(\varphi)\delta(x+1) + \lambda_R(\varphi)\delta(x-1).$$

The general stationary state for the hamiltonian H_0 can obviously be written as a linear combination of separable terms $|k\rangle|m\rangle$, where

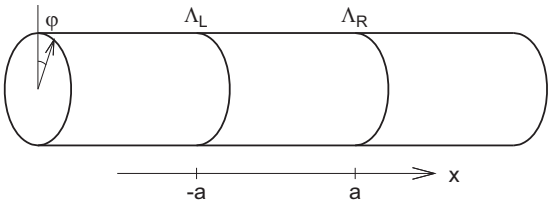

Fig. 2. Alternative interpretation of the model – electron motion on a surface of a cylinder with double barrier.

(in coordinate representation)

$$\phi_m(\varphi) \equiv \langle \varphi | m \rangle = \frac{1}{\sqrt{2\pi}} e^{im\varphi},$$

$$\langle x | k \rangle = \frac{1}{\sqrt{2\pi}} e^{ikx},$$

and the quantum numbers m and k, are related to the energy through the relation:

$$E = \frac{1}{2}k^2 + \frac{m^2}{2I}. \tag{3}$$

In this work we will treat the collision of the electron with momentum $k > 0$ (electron coming from the left) and the junction initially in the ground vibrational state $m_i = 0$. The full wave function of this scattering problem can be found as the unique solution of the Lippmann–Schwinger equation:

$$|\psi\rangle = |k\rangle |m_i\rangle + G_0(E) V |\psi\rangle, \tag{4}$$

where the retarded Green's function $G_0(E)$ is given by the standard expression $(E^+ - H_0)^{-1}$. It is convenient to expand the wave function $|\psi\rangle$ in the free rotor basis $\phi_m(\varphi)$

$$\psi(x, \varphi) = \sum_m \psi_m(x) \phi_m(\varphi), \tag{5}$$

where the sum runs over $m = 0, \pm 1, \pm 2, \ldots, \pm M$. The maximum value of the angular momentum M is in principle infinite, but for the practical calculation we fix it to some sufficiently large finite value (see below). The Green's function $G_0(E)$ is diagonal in this basis, with the diagonal elements given by the one dimensional free-particle Green's function:

$$\langle x, m | G_0(E) | x', m' \rangle = \frac{1}{ik_m} \delta_{mm'} e^{ik_m |x - x'|}. \tag{6}$$

The value of the momentum $k_m = \pm \sqrt{2E - m^2/I}$ follows from the energy conservation relation (3). For the closed channels with $m > \sqrt{2IE}$, we must choose the value with $\mathrm{Im}\, k_m > 0$, in order to get the retarded Green's function, while for the open channels k_m is the positive real number. The Lippmann–Schwinger equation (4) then reads (expansion in the free rotor basis)

$$\psi_m(x) = \frac{1}{2\pi} \delta_{mm_i} e^{ik_m x} + \frac{1}{ik_m} \sum_{m'} \left\{ e^{ik_m |x+1|} \Lambda^{(L)}_{mm'} \psi_{m'}(-1) + e^{ik_m |x-1|} \Lambda^{(R)}_{mm'} \psi_{m'}(1) \right\}, \tag{7}$$

where we have introduced the matrix elements

$$\Lambda^{(l)}_{mm'} = \langle m | \lambda_l | m' \rangle = \frac{1}{2\pi} \int_0^{2\pi} \lambda_l(\varphi) e^{i(m' - m)\varphi} \mathrm{d}\varphi, \tag{8}$$

expressing the angular dependence of the barrier height in the free rotor basis. Notice that this form of the Lippmann–Schwinger equation fixes the whole x-dependence of the wave function based on the knowledge of the wave function in the barrier points $x = \pm 1$. Substituting these two values of x in (7), we get the linear system of equations for $2(2M+1)$ components of the vectors $\Psi_\pm \equiv \{\psi_m(\pm 1)\}_{m=-M,\ldots,M}$, which can be written in the matrix form:

$$\begin{pmatrix} \Psi_- \\ \Psi_+ \end{pmatrix} = \begin{pmatrix} \Phi^{(i)}_- \\ \Phi^{(i)}_+ \end{pmatrix} + \begin{pmatrix} G_{--} & G_{-+} \\ G_{+-} & G_{++} \end{pmatrix} \begin{pmatrix} \Lambda^{(L)} & 0 \\ 0 & \Lambda^{(R)} \end{pmatrix} \begin{pmatrix} \Psi_- \\ \Psi_+ \end{pmatrix}, \tag{9}$$

where we have introduced the diagonal matrices $G_{++} = G_{--} \equiv \mathrm{diag}\{1/ik_m\}$, $G_{+-} = G_{-+} \equiv \mathrm{diag}\{(1/ik_m) e^{2ik_m}\}$ and each vector $\Phi^{(i)}_\pm$ has only one nonzero element $e^{\pm} ik_m/\sqrt{2\pi}$ for $m = m_i$. The equation can be solved directly by matrix inversion. The T-matrix elements $T^+_{mm_i}$ for transmission and $T^-_{mm_i}$ for reflection with the junction left in the final state $m = m_f$ then read

$$T^+_{mm_i} = \frac{1}{\sqrt{2\pi}} \sum_{m'} [e^{ik_m} \Lambda^{(L)}_{mm'} \psi_{m'}(-1) + e^{-ik_m} \Lambda^{(R)}_{mm'} \psi_{m'}(1)], \tag{10}$$

$$T^-_{mm_i} = \frac{1}{\sqrt{2\pi}} \sum_{m'} [e^{-ik_m} \Lambda^{(L)}_{mm'} \psi_{m'}(-1) + e^{ik_m} \Lambda^{(R)}_{mm'} \psi_{m'}(1)]. \tag{11}$$

The corresponding transmission and reflection probabilities are then expressed as a square of the S-matrix elements

$$P^T_{mm_i} = \left| \delta_{mm_i} - \frac{2\pi i}{\sqrt{k_m k_{m_i}}} T^+_{mm_i} \right|^2, \tag{12}$$

$$P^R_{mm_i} = \left| \frac{2\pi i}{\sqrt{k_m k_{m_i}}} T^-_{mm_i} \right|^2. \tag{13}$$

The total probabilities are simply the sums over all the outgoing channels

$$P_l = \sum_m P^l_{mm_i}. \tag{14}$$

It is also possible to calculate the mean value of the angular momentum after the collision

$$\langle m \rangle = \sum_m m (P^L_{mm_i} + P^R_{mm_i}). \tag{15}$$

3. Discussion and the results

We have shown how to calculate the transmission and the reflection probabilities in the previous section. It is simple to implement the method. The only approximation made is the expansion of the φ-dependence of the wavefunction in the Fourier basis, which is limited to finite number of terms. Since this dependence is smooth, the fast convergence with the parameter M is expected. We checked that the accuracy better then 10 decimal digits is achieved with $M = 50$, which is the value used throughout this paper.

Before showing the results for the full calculation we will discuss the possible regimes of the transport in the model. This analysis is based on the typical energy and time-scales.

3.1. 1D double barrier scattering

The typical time-scales for the torsional vibrations are inversely proportional to the spacing of the vibrational levels $\Delta E_m \sim (1/2I)$. For low collision energies $E \ll \Delta E_m$ or small moment of inertia I the torsional vibrations are completely frozen and we end up with the simplified model of scattering of electron in 1D from the double barrier described by hamiltonian

$$H_{1D} = -\frac{1}{2}\frac{\partial^2}{\partial x^2} + \overline{\lambda}_L \delta(x+1) + \overline{\lambda}_R \delta(x-1). \tag{16}$$

The constants $\overline{\lambda}_L$, $\overline{\lambda}_R$ are the mean values of the functions $\lambda_l(\varphi)$ averaged over the initial vibrational state

$$\overline{\lambda}_\alpha = \langle m_i | \lambda_\alpha(\varphi) | m_i \rangle = \int |\phi_{m_i}(\varphi)|^2 \lambda_\alpha(\varphi) \mathrm{d}\varphi. \tag{17}$$

The scattering of the electron in this case can be solved with the same method as above, except that the quantum number $m = m_i$ is conserved, i.e. the column vectors $\Psi_\pm$ reduce to single numbers and the system of Eqs. (9) reduces to two equations, that can be solved by hand. This procedure leads to the transmission and the reflection probabilities

$$P_T = \left| \frac{k^2}{\overline{\lambda}_L \overline{\lambda}_R e^{4ik} - (\overline{\lambda}_L - ik)(\overline{\lambda}_R - ik)} \right|^2 \tag{18}$$

$$P_R = \left| \frac{\overline{\lambda}_L e^{-2ik}(\overline{\lambda}_R - ik) - \overline{\lambda}_R e^{2ik}(\overline{\lambda}_L + ik)}{\overline{\lambda}_L \overline{\lambda}_R e^{4ik} - (\overline{\lambda}_L - ik)(\overline{\lambda}_R - ik)} \right|^2 . \tag{19}$$

The results for the one dimensional case and for $\overline{\lambda}_L = \overline{\lambda}_R = 2.0$ are shown in Fig. 3 (solid line). The shape of the transmission function is typical for the double barrier tunneling, characterized by multiple resonance peaks, which become broader for higher energies.

Before going any further we will discuss briefly the width and the position of these peaks. They can be found from the analysis of the position of the S-matrix poles in the complex energy plain. In our case these peaks are related to complex zeros of the denominator in (18). As a rough estimate we can take the values $k_R = n\pi/2$, for $n = 1, 2, \ldots$, which are the poles of (18) in the limit $\lambda_\alpha \to \infty$. This approximation gives the position of the resonance peaks at $E_1 = \pi^2/8 \doteq 1.2$ and $E_2 = \pi^2/2 \doteq 4.9$. Notice that these energies coincide with the eigen-energies of the particle trapped in the infinitely deep box located in interval $(-1, 1)$. The peaks in Fig. 3 are located at little lower energies. It is not difficult to calculate the exact position of the poles of (18) numerically, or to find few more terms of the perturbation series of k_R in powers of $1/\lambda_\alpha$. We will concentrate on the first pole (corresponding to the first peak) and denote its position in complex energy plane $E = 1/2k_R^2 = E_r - i/2\Gamma$. In the symmetric case $\lambda_L = \lambda_R \equiv \lambda$ the perturbation calculation in the second order in $1/\lambda$ gives

$$E_r = \frac{\pi^2}{8}\left(1 - \frac{1}{\lambda} + \frac{3}{4}\frac{1}{\lambda^2}\right), \tag{20}$$

$$\Gamma = \frac{\pi^3}{16\lambda^2}. \tag{21}$$

The resulting value $E_r = 0.85$ corresponds well to the position of the peak in Fig. 3, but the width $\Gamma = 0.48$ is overestimated by factor of 2. This is no surprise since the formula (21) is the first term in the expansion in $1/\lambda$, which is not expected to converge fast for $\lambda = 2$. Still we have got a good order of magnitude estimate, which will even be better for higher λ.

Fig. 3 also shows results of the full calculation for small moments of inertia. The transmission function $P_T(E)$ for $I = 0.1$ (dotted curve) follows closely the exact formula for the 1D case. For higher value $I = 0.5$ (long dashes) the transmission starts to deviate from the 1D formula in the region of the second peak. This is consequence of the fact that the 1D approximation is expected to work better at low energies. The lowest excited state of torsional vibrations now appears as a small peak at energy of 1.8, which is $1/2I$ above the main resonance peak. Even the shape

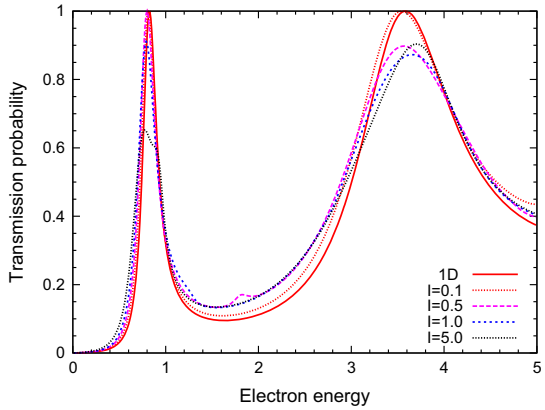

Fig. 3. Typical transmission function for the one dimensional model (solid line) and the deviations for moderately coupled torsional vibrations $\beta/\alpha = 0.5$ and for small moments of inertia $I = 0.1, 0.5, 1.0, 5.0$.

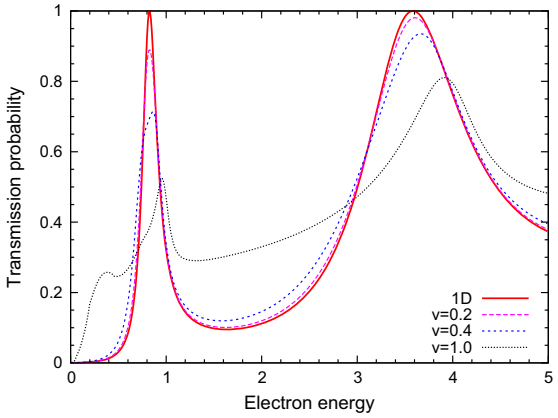

Fig. 4. Transmission functions for increasingly large coupling $v = 0, 0.2, 0.4, 1.0$ and for moderate moment of inertia $I = 10$.

of the main resonance peak at $E = 0.8$ becomes deformed for higher moments of inertia $I = 1.0, 5.0$.

The values of I used in the previous discussion are still far lower than the realistic values expected for real molecules (thousands). The usefulness of the 1D approximation, understood as the low energy approximation, may therefore be questionable. On the other hand, the 1D approximation also works well in the limit of the small vibrational coupling. The extreme case is considering no coupling at all, which is achieved by setting $\beta_l = 0$ in our model (see (2)), i. e. $\lambda_l(\varphi) = \overline{\lambda}_l$, independent of φ. The kinetic energy of the torsional vibrations $-(1/2I)(\partial^2/\partial\varphi^2)$ then commutes with the full Hamiltonian (1) and the quantum number $m = m_i$ is conserved exactly in the collision.

Fig. 4 compares the transmission function for the full calculation with the results of 1D model again. This time the parameters of the model are $\alpha_L = \alpha_R = 2.0$, $\varphi_0 = 1.0$, $I = 10$ and $\beta_L = \beta_R = \beta$. The vibrational coupling is characterized by number $v = \beta/\alpha$. The case $v = 0$ represents the uncoupled system and the transmission coincides with the analytic 1D formula where $\lambda = \alpha$. Increasing the coupling parameter v, we start to deviate more and more form the 1D case. For $v = 1$ the simple picture of double barrier scattering that created the two sharp peaks breaks.

3.2. Chase approximation

In the preceding section we presented the 1D model as the low-energy limit or the low-coupling limit of the full problem. When the electron interaction with vibrational degrees of freedom of the molecule is considered, the most important role of the 1D model lies in its potential to describe the limit of the heavy molecule $I \to \infty$. The timescale of the torsional vibrations for a very heavy molecule is supposed to be long. If the scattering of the electron is happening on a much shorter timescale, we can expect that the vibrational coordinate φ is fixed during the course of the collision. The transmission function $p_T(\varphi, E)$ can thus be calculated using analytic formula (18) for 1D model using $\lambda_l(\varphi)$ for the fixed value of φ, which has to be averaged over the distribution of the angles $|\phi_{m_i}(\varphi)|^2$ in the initial state

$$P_T^{Chase}(E) = \int p_T(\varphi, E)|\phi_{m_i}(\varphi)|^2 \, \mathrm{d}\varphi \tag{22}$$

The same approach is known in the description of electron scattering from the molecules in gas phase as the Chase approximation [18].

The performance of this approximation is shown in Fig. 5. The parameters of the model are the same as in Fig. 4 for $v = 1$ and for increasing values of $I = 1, 5, 10, 100$. It is obvious that the curves

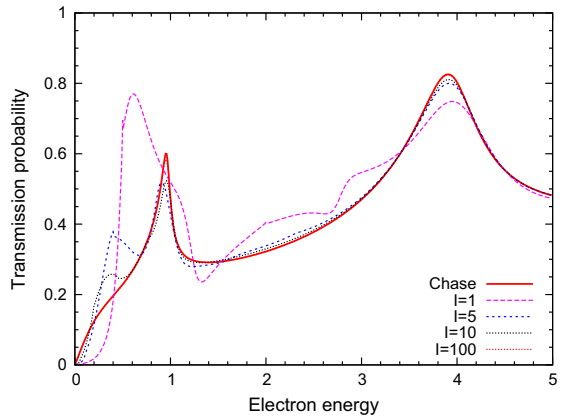

Fig. 5. Transmission function for strong coupling $v=1.0$ and the Chase approximation as the limit for large moment of inertia (curve for $I=100$ overlaps with Chase approximation within the linewidth).

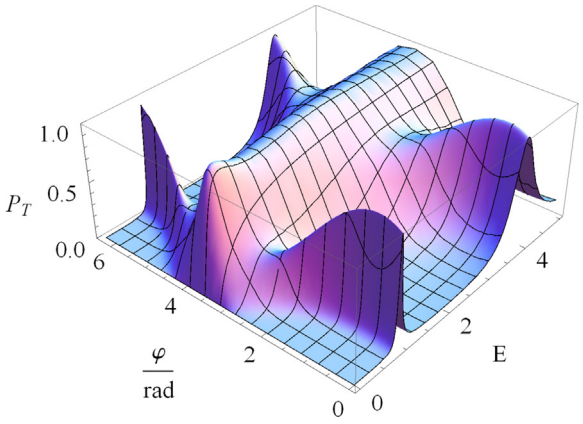

Fig. 6. Transmission function for 1D model as a function of angle φ. Chase approximation in Fig. 5 is average of this function over all angles.

gradually approach Chase approximation (22). In general, this approximation performs better for larger energies, as expected from the argument about the time-scales above. To understand the shape of the limit curve we also show the plot of function $p_T(\varphi, E)$ in Fig. 6. Let us remind that it is $\phi_{m_i}(\varphi) = const.$ in our calculation. The Chase approximation is thus simply average of the function $p_T(\varphi, E)$ over all angles.

3.3. Local complex potential approximation

Introducing the Chase approximation in the previous section we omitted to give more rigorous condition for its validity. The relevant timescales can be estimated in the resonance regime $\lambda \gg 1$. The width Γ of the resonance peak is then well approximated by formula (21). The timescale for electron tunneling through the molecular junction is inversely proportional to Γ. The Chase approximation is thus expected to work well for $\Gamma \sim \lambda^{-2} \gg I^{-1}$. Problems are expected for very narrow resonances. We demonstrate this in Fig. 7. The transmission function is shown in the vicinity of the main resonance peak for the case of $\alpha_L = \alpha_R = 20$, $v=0.5$ and for increasing values of I. The convergence to Chase approximation is slow and considerable deviations are observed even for $I=500$. It is clear that for very narrow resonances the Chase approximation will fail even for very heavy molecules.

This behavior is well known from electron scattering from molecules in the gas phase [16]. It is possible to construct an alternative approximation in this case, which is based on the fact that the transmission function is dominated by a single resonance. This approach was first proposed to describe the many body discrete states coupled to a continuum through configuration interaction [20,26–28], but Domcke [29] have shown that it can also be applied to single-particle potential scattering.

In the case of a two dimensional potential model, it is possible to construct the discrete-state-in-continuum model from first principles [30], but in this work we prefer much simpler approach, the local complex potential (LCP) approximation, which is applicable in the case of narrow resonance peaks far from threshold (i. e. $v<1$; $\Gamma \ll E_r$). The construction of the discrete state model proceeds as follows. We parameterize the electron dynamics for each fixed vibrational coordinate φ by three parameters: the resonance energy $E_r(\varphi)$ and the partial resonance widths $\Gamma_l(\varphi)$ describing the coupling strength of the discrete state relative to left ($l=L$) and the right ($l=R$) electrode. These parameters are found fitting (for each φ separately) the 1D transmission function $p_T(\varphi, E)$ to the famous Breit–Wigner formula:

$$p_T(E) = \frac{\Gamma_L \Gamma_R}{(E-E_r)^2 + \left[\frac{1}{2}(\Gamma_L+\Gamma_R)\right]^2}. \tag{23}$$

Knowing the parameterization of the discrete state model the transmission function can be constructed from the formula (analogical formula is known in electron scattering from molecules in gas phase [31,16])

$$P^{T,LCP}_{m_f m_i} = \left| \langle m_f | \sqrt{\Gamma_R} \left[E + \frac{1}{2I}\frac{\partial^2}{\partial\varphi^2} - E_r + \frac{i}{2}[\Gamma_L+\Gamma_R] \right]^{-1} \sqrt{\Gamma_L} | m_i \rangle \right|^2. \tag{24}$$

We have to keep in mind that the quantities E_r, Γ_l in this expression are functions of φ, i.e. they are matrices in the free rotor basis $|m\rangle$.

To show the performance of the LCP approximation we have calculated the full transmission functions for the same model as in Fig. 7. The transmissions for LCP approximation (short dashes) are compared with the full calculation (solid line) and with the Chase approximation (long dashes) in Fig. 8 in logarithmic scale. Observe that the LCP approximation gives perfect description of the shape of the resonance peak (within the linewidth), but it fails to reproduce the background transmission away from resonance. This is minor difficulty, since the background transmission is very small and it can well be reproduced by the Chase approximation instead. To conclude the Chase approximation combined with LCP model gives a very good understanding of the transmission functions in resonance regime.

3.4. Excitation of the torsional vibrations

We have studied only the total transmission probabilities so far. The individual contributions (12) are plotted in Fig. 9. The LCP model gives these contributions directly (24). The Chase approximation (22) has to be modified for this purpose

$$P^{T,Chase}_{m_f m_i}(E) = \left| \int \phi_{m_f}(\varphi)^* S_T(\varphi, E) \phi_{m_i}(\varphi)\, \mathrm{d}\varphi \right|^2, \tag{25}$$

where S_T is the S-matrix element for the transmission (the expression inside the absolute value in Eq. (18)). Resulting individual transmissions in the Chase and LCP approximations are also shown in Fig. 9. The transmission function is shown for three values of final angular momentum $m_f=0$, 1, 2. We observe the same behavior as for the total transmissions. The LCP approximation works very well inside the resonance peak, while the background transmission is very well described in Chase approximation. We also see that the excitation of the torsional vibrations is very efficient. The contributions $0\to1$, $0\to2$ for transmission functions including the

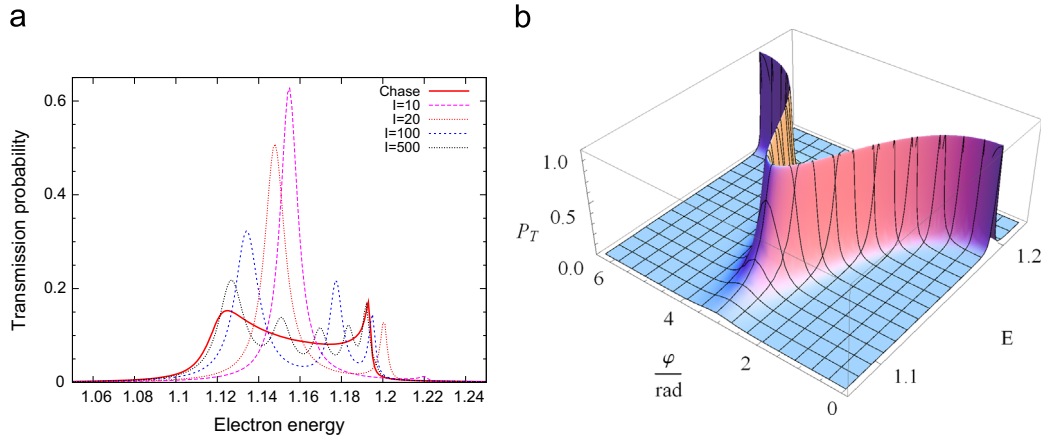

Fig. 7. Transmission function (left) in the case of narrow resonance $\alpha=20$ and moderate coupling $\nu=0.5$. The Chase approximation (solid line) is not quite reached even for large moment of inertia $I=500$. The reason for broadening of the peak in Chase approximation can be understood from φ-dependence of 1D transmission (right).

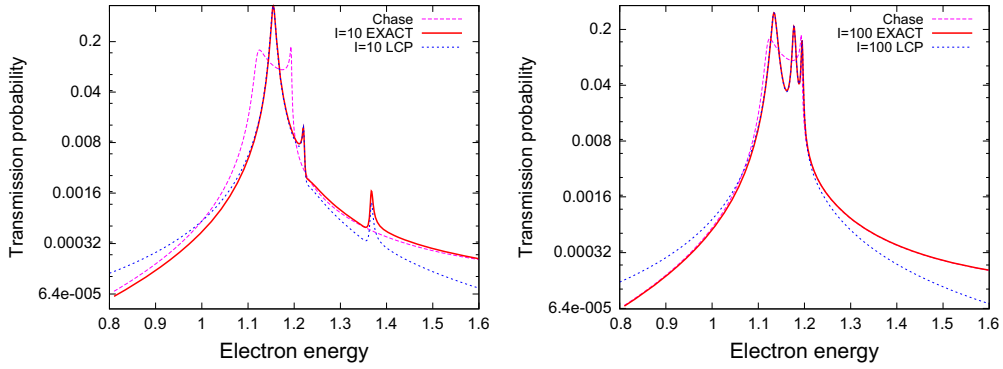

Fig. 8. Transmission functions in logarithmic scale for the energies near the narrow resonance peak ($\alpha=20$, $\nu=0.5$). Performance of Chase approximation and the LCP model is shown for two values of moment of inertia $I=10$ and 100.

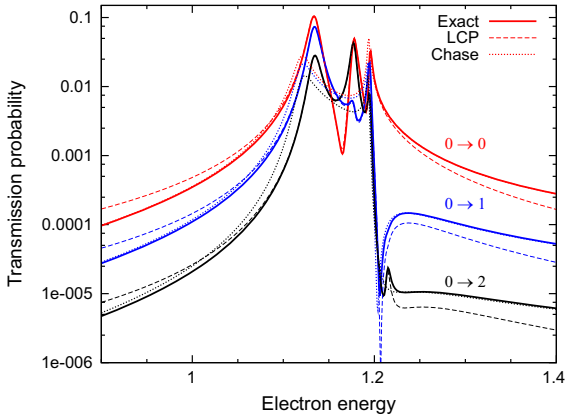

Fig. 9. Individual transmission functions for different final states of the torsional vibration mode ($m=0,1,2$) in the logarithmic scale for the energies near the narrow resonance peak ($\alpha=20$, $\nu=0.5$). The performance of Chase approximation (dots) and the LCP model (dashes) for $I=100$ is shown.

excitation of the first and second state respectively reach the peak values comparable to the elastic contribution $0\to0$. This is consequence of the fact that the typical lifetime of the resonance $1/\Gamma\simeq200$ estimated from formula (21) is of comparable size to the typical period $\sim2\pi I$ of the torsional vibrations for the chosen model.

The excitation of the torsional vibrations becomes asymmetric for the chiral model with $\phi_0\neq0 \bmod \pi$. It is demonstrated in Fig. 10. The mean value of the angular momentum (15) becomes relatively high near the resonance peak. The direction of the rotations (given by sign of $\langle m\rangle$) can be controlled by selecting the value of ϕ_0. In the example selected in the figure the two values correspond to ϕ_0 and $\pi-\phi_0$. The direction of the torsional vibrations can thus be inverted by interchanging the left and right electrodes, i.e. by inverting the direction of the current.

3.5. Threshold structures in strong coupling regime

The regime with $\nu>1$ is interesting by itself. We cannot apply the LCP approximation in this regime, even for large value of α, since the resonance is transformed into bound state with changing value of φ. This case can still be treated with the model of discrete state in continuum [16,30], but both the nonlocality and energy dependence of Γ cannot be neglected. It is beyond scope of the present article to study this approximation. We will restrict to the presentation of some interesting phenomena in this regime with the full calculation.

We show the total transmission function for $\alpha=1$, $\nu=5$ and $\phi_0=\pi$ in Fig. 11. The transmission is shown for three values of the angular momentum and the Chase approximation is also shown. The Chase approximation describes the transmission quite well for the energies $E>1$. The transmission for the 1D model is also shown in Fig. 12. Comparing the two figures we understand the nature of the main peak at $E\simeq1.3$ and also the weak peak at $E\simeq0.7$. The exact curves also exhibit pronounced narrow structures at small energies, which cannot be comprehended within Chase approximation.

To understand better nature of these structures we expand the low-energy region in Fig. 13. Only the transmission for $I=100$ is shown there in logarithmic scale. There is a narrow peak at

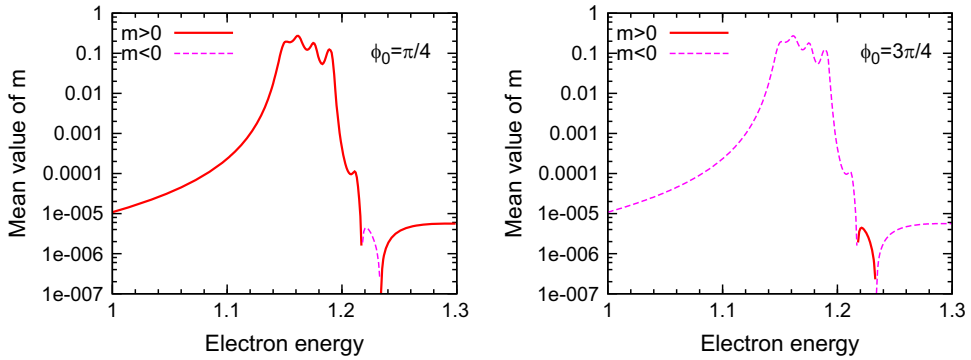

Fig. 10. The mean value of the angular momentum m after the collision. The parameters are the same as for Fig. 9 except for ϕ_0; its values are shown in each panel.

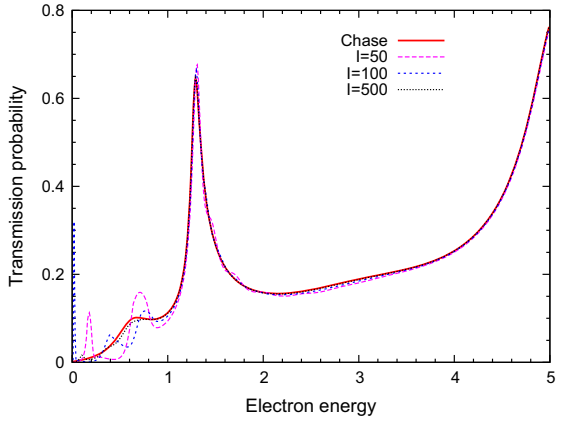

Fig. 11. Transmission function for strong coupling $v=5.0$, $\alpha=1$ and the Chase approximation for three moments of inertia as indicated in the figure.

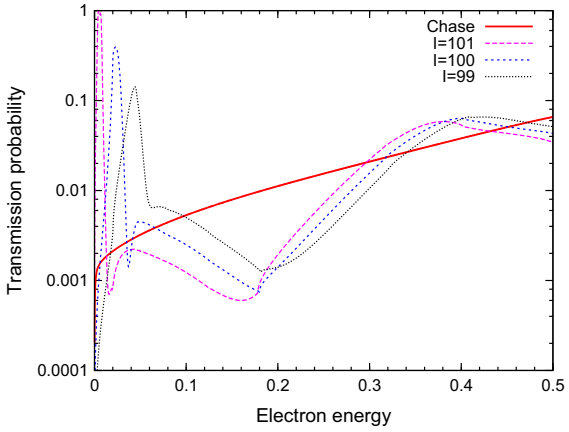

Fig. 13. Detail of threshold structures from Fig. 11. Only curve with $I=100$ is enlarged and compared with $I=99$ and $I=101$ to show the sensitivity of the structures.

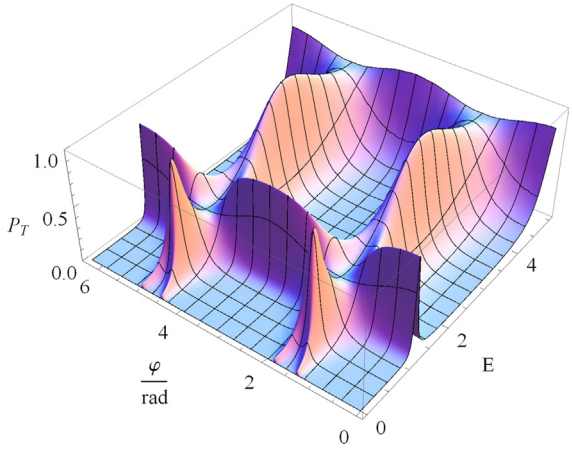

Fig. 12. Transmission function for 1D model as a function of angle φ. Chase approximation in Fig. 11 is average of this function over all angles.

$E\simeq 0.02$. Both the position and the size of this peak are extremely sensitive to the parameters of the model. To show this we included a calculation with slightly perturbed angular momentum $I=100\pm 1$. The peak is shifted towards lower energies with increasing mass and its maximum increases until it reaches 1, i.e. the maximum value permitted by unitarity. Closer investigation shows that the peak origins in the strong coupling of the electronic and vibrational motion. Functions $\lambda_l(\varphi)$ (see Eq. (2) in the first section) attain negative values for $v>1$. The delta barriers are then transformed into potential wells and they can support several vibrational states. The peaks in Fig. 13 capture the resonance which transforms into such bound state when the mass (momentum of inertia I plays the role of the mass) of the system is increased. The large size of the peak is consequence of the existence of the pole of the S-matrix in the vicinity of the origin. Further increase of the mass would destroy the peak completely but the second peak at $E\simeq 0.4$ would be shifted to the vicinity of the origin. We checked that for $I=120$ such narrow peak is again present near the origin.

Similar behavior resulting from coupled electronic and vibrational degrees of freedom influenced by threshold phenomena is also observed in electron collisions with molecules [32,33].

3.6. Role of the molecular vibrational potential

The vibrational structure of the molecule has so far been modeled with the free rotor here and we did not consider the potential energy of the molecular vibrations in our model (1). It is easy to add the term $V_0(\varphi)$ in (1) and in the definition of the Hamiltonian H_0 at the beginning of Section 2 to include the potential energy of torsional vibrations. This changes the calculation procedure only slightly. We have to modify the expansion of the wavefunctions by replacing the free rotor basis $\phi_m(\varphi)$, with the eigenstates $\tilde{\phi}_m(\varphi)$ of the operator:

$$-\frac{1}{2I}\frac{\partial^2}{\partial\varphi^2}+V_0(\varphi).$$

Its eigenenergies E_m will enter Eq. (3) instead of the factor $m^2/2I$ and also the momenta $k_m=\pm\sqrt{2(E-E_m)}$ have to be calculated from these energies. The matrix elements of the barrier heights (8)

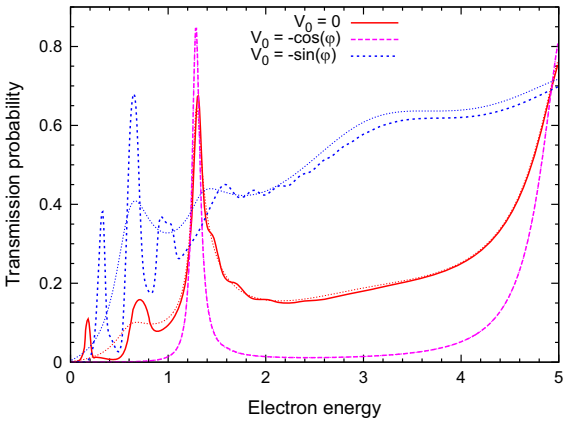

Fig. 14. Transmission functions for nontrivial vibrational potential $V_0(\varphi)$. The red solid line is the same as in figure 11 ($I=50$) for comparison. The Chase approximation, for each case, is also shown with dots.

have to be calculated in this new basis

$$\Lambda^{(l)}_{mm'} = \int_0^{2\pi} \tilde{\phi}_m(\varphi)^* \lambda_l(\varphi) \tilde{\phi}_{m'}(\varphi)\, \mathrm{d}\varphi. \tag{26}$$

All the other computational details remain the same.

We do not intend to investigate the effect of the molecular vibrational potential in this paper in systematic way. To show the effect of the vibrational potential on the results we just discuss the transmission function for the same model as in the last section with $I=50$. This transmission function is replotted in Fig. 14 with red solid line. Also shown is the transmission with the vibrational potential $V_0 = -\cos\varphi$ (purple long dashes) and $V_0 = -\sin\varphi$ (blue short dashes). The ground state of the former is localized close to its minimum at $\varphi = 0$, while the later potential has the minimum and the ground state localized at $\varphi = \pi/2$. The transmission in the former case is characterized with sharp resonance peak but no notable vibrational structure, the later case exhibits a large nonresonant background and many structures. This is easily understandable since the vibrational potential V_0 confines the system in the area where functions $\lambda_L(\varphi)$ and $\lambda_R(\varphi)$ are stationary or fast changing respectively. The former case is thus in the resonant regime only weakly coupled to vibrations while the later case is in the strongly coupled nonresonant regime. This is also reflected in the applicability of the Chase approximation (shown as dotted lines in Fig. 14). The approximation works perfectly in the weakly coupled regime (the dotted line is indistinguishable from the full calculation plotted with long dashed curve), while the approximation is not capable to describe correctly the peaks resulting from the vibrational coupling marked with short dashes. In the case of the free rotor, studied in the previous section, the wave function is completely delocalized through all values of φ and the behavior of the transmission function is somewhere between these two extreme cases.

In general we can state that the results of the previous sections apply also for the case with nonzero V_0, but we have to consider the restriction that V_0 imposes on the values of φ probed in the collision. The potential V_0 above, with the sine/cosine shape serves as an example of potential with single minimum, and the results are very close to what would be obtained with the harmonic potential, which is more frequently used to model the molecular vibrations.

4. Conclusions and future prospects

We have discussed the transmission functions for the inelastic tunneling of an electron through the double barrier structure in molecular junction with coupling to torsional vibrations. The exact transmission functions were compared to various approximation methods, which allow separation of the full transmission problem into sequential calculation for electronic and vibrational dynamics.

Particularly useful is the approximation of frozen vibrations (analog of Born–Oppenheimer approximation for the scattering), which corresponds to 1D approximation in our two dimensional model. We have shown how this approximation may help to give an interpretation to a structures in the transmission functions in the limit of small energies $E \ll 1/2I$ or small vibrational coupling $\nu = \beta/\alpha \ll 1$.

Even more important case in which the approximation of frozen vibrations takes part is the Chase approximation, giving the full transmission as an average of the 1D analytic formula (i.e. purely electronic transport with fixed nuclei in our model) over the vibrational wave-functions of the molecule. This approximation is exact in the limit of infinitely heavy molecule $I \to \infty$. The range of applicability of this approximation has been studied in more details here. We have shown that the approximation fails in the resonant regime, where it can be replaced by the projection-operator methods, which we demonstrated on the LCP approximation. We have also shown that the combination of the LCP approximation and the Chase approximation can be used to accurately represent the excitation functions of the different vibrational states in the junction.

For strong vibrational coupling $\nu > 1$ the LCP approximation is not well defined. It can be replaced by the method on nonlocal resonance model [16]. It is beyond the scope of this paper to construct and study this approximation, but it can provide the insight in the nature of structures observed in the strong coupling regime.

If the chiral symmetry of the junction is broken the molecular junction can be used as molecular motor [34]. We show this behavior also on the current model, i.e. we demonstrate that the sign of the average angular momentum of the junction can be controlled by the direction of the current passing through the junction.

Acknowledgments

This work was supported by grant GACR 208/10/1281. L.G. gratefully acknowledges the support by the Faculty of Mathematics and Physics of Charles University in Prague through the "Student faculty grant".

References

[1] R.J. Hath, Ann. Rev. Mater. Res. 39 (2009).
[2] M. Reed, C. Zhou, C. Muller, T. Burgin, J. Tour, Science 278 (1997) 252.
[3] M. Ratner, Nat. Nanotechnol. 8 (2013) 378.
[4] M. Tsutsui, M. Taniguchi, Sensors 12 (2012) 7259.
[5] A. Nitzan, M.A. Ratner, Science 300 (2003) 1384.
[6] T. Seideman, Current-driven phenomena in nanoelectronics, Pan Stanford Publishing, 2010.
[7] N.A. Zimbovskaya, M.R. Pederson, Phys. Rep. 509 (2011) 1.
[8] T. Frederiksen, M. Paulsson, M. Brandbyge, A.-P. Jauho, Phys. Rev. B 75 (2007) 205413.
[9] S. Ulstrup, T. Frederiksen, M. Brandbyge, Phys. Rev. B 86 (2012) 245417.
[10] K.F. Albrecht, H. Wang, L. Muhlbacher, M. Thoss, A. Komnik, Phys. Rev. B 86 (2012) 081412(R).
[11] H. Wang, M. Thoss, J. Chem. Phys. 138 (2013) 134704.
[12] K. Kaasbjerg, T. Novotný, A. Nitzan, Phys. Rev. B 88 (2013) 201405(R).
[13] T. Novotný, J. Comput. Electron. 12 (2013) 375.
[14] T. Seideman, J. Phys.: Condens. Matter 15 (2003) R521.
[15] M. Čížek, M. Thoss, W. Domcke, Phys. Rev. B 70 (2004) 125406.
[16] W. Domcke, Phys. Rep. 208 (1991) 97.
[17] P. Čársky, R. Čurík (Eds.), Low-Energy Electron Scattering from Molecules Biomolecules and Surfaces, CRC Press, Boca Raton, FL, 2012.
[18] D.M. Chase, Phys. Rev. 104 (1956) 838.
[19] A. Troisi, M.A. Ratner, A. Nitzan, J. Chem. Phys. 118 (2003) 6072.

[20] H. Feshbach, Ann. Phys. (NY) (1958) 357.
[21] M. Čížek, K. Houfek, Chapter 4 (p. 91), in: P. Čárský, R. Čurík (Eds.), Low-Energy Electron Scattering from Molecules, Biomolecules and Surfaces, 2012, p. 91.
[22] M. Čížek, M. Thoss, W. Domcke, Czech. J. Phys. 55 (2005) 189.
[23] L. Venkataraman, J.E. Klare, C. Nuckolls, M.S. Hybertsen, M.L. Steigerwald, Nature 442 (2006) 904.
[24] F. Pauly, J.K. Viljas, J.C. Cuevas, G. Schon, Phys. Rev. B 77 (2008) 155312.
[25] M. Bürkle, J.K. Viljas, D. Vonlanthen, A. Mishchenko, G. Schon, M. Mayor, T. Wandlowski, F. Pauly, Phys. Rev. B 85 (2012) 075417.
[26] J.C.Y. Chen, Phys. Rev. 148 (1966) 66.
[27] T.F. O'Malley, Phys. Rev. 150 (1966) 14.
[28] J.N. Bardsley, J. Phys. B 1 (1968) 349.
[29] W. Domcke, Phys. Rev. A 28 (1983) 2777.
[30] K. Houfek, T.N. Rescigno, C.W. McCurdy, Phys. Rev. A 77 (2008) 012710.
[31] A. Herzenberg, J. Phys. B 1 (1968) 548.
[32] J. Fedor, C. Winstead, V. McKoy, M. Čížek, K. Houfek, P. Kolorenč, J. Horáček, Phys. Rev. A 81 (2010) 042702.
[33] M. Čížek, J. Horáček, M. Allan, W. Domcke, Czech. J. Phys. 52 (2002) 1057.
[34] I.A. Pshenichnyuk, M. Čížek, Phys. Rev. B 83 (2011) 165446.